A Novel Diamond-like Carbon based photocathode for PICOSEC Micromegas detector

X. Wang,[a,b] **Y. Zhou,**[a,b,1] **R. Aleksan,**[c] **Y. Angelis,**[d] **J. Bortfeldt,**[e] **F. Brunbauer,**[f] **M. Brunoldi,**[g,h] **E. Chatzianagnostou,**[d] **J. Datta,**[i] **K. Degmelt,**[j] **G. Fanourakis,**[k] **D. Fiorina,**[g,h] **K.J. Floethner,**[f,l] **M. Gallinaro,**[m] **F. Garcia,**[n] **I. Giomataris,**[c] **K. Gnanvo,**[j] **F.J. Iguaz,**[c] **D. Janssens,**[f] **A. Kallitsopoulou,**[c] **M. Kovacic,**[o] **B. Kross,**[j] **P. Legou,**[c] **M. Lisowska,**[f,p] **J. Liu,**[a,b] **J. Liu,**[l,q] **I. Maniatis,**[f,c] **J. McKisson,**[j] **Y. Meng,**[a,b] **H. Muller,**[f,q] **E. Oliveri,**[f] **G. Orlandini,**[f,r] **A. Pandey,**[j] **T. Papaevangelou,**[c] **M. Pomorski,**[s] **L. Ropelewski,**[f] **D. Sampsonidis,**[d,t] **L. Scharenberg,**[f] **T. Schneider,**[f] **L. Shang,**[u] **M. Shao,**[a,b] **L. Sohl,**[c] **M. van Stenis,**[f] **Y. Tsipolitis,**[v] **S.E. Tzamarias,**[d,t] **A. Utrobicic,**[w] **I. Vai,**[g,h] **R. Veenhof,**[f] **P. Vitulo,**[g,h] **S. White,**[f,g] **W. Xi,**[j] **and Z. Zhang**[a,b]

[a] *State Key Laboratory of Particle Detection and Electronics, University of Science and Technology of China, Hefei 230026, China*

[b] *Department of Modern Physics, University of Science and Technology of China, Hefei 230026, China*

[c] *IRFU, CEA, Université Paris-Saclay, F-91191 Gif-sur-Yvette, France*

[d] *Department of Physics, Aristotle University of Thessaloniki, University Campus, GR-54124, Thessaloniki, Greece*

[e] *Department for Medical Physics, Ludwig Maximilian University of Munich, Am Coulombwall 1, 85748 Garching, Germany*

[f] *European Organisation for Nuclear Research (CERN), CH-1211, Geneve 23, Switzerland*

[g] *Dipartimento di Fisica, Università di Pavia, Via Bassi 6, 27100 Pavia (IT)*

[h] *INFN Sezione di Pavia, Via Bassi 6, 27100 Pavia (IT)*

[i] *Stony Brook University, Dept. of Physics and Astronomy, Stony Brook, NY 11794-3800, USA*

[j] *Jefferson Lab, 12000 Jefferson Avenue, Newport News, VA 23606, USA*

[k] *Institute of Nuclear and Particle Physics, NCSR Demokritos, GR-15341 Agia Paraskevi, Attiki, Greece*

[l] *Helmholtz-Institut für Strahlen- und Kernphysik, University of Bonn, Nußallee 14–16, 53115 Bonn, Germany*

[m] *Laboratório de Instrumentacão e Física Experimental de Partículas, Lisbon, Portugal*

[n] *Helsinki Institute of Physics, University of Helsinki, FI-00014 Helsinki, Finland*

[o] *Faculty of Electrical Engineering and Computing, University of Zagreb, 10000 Zagreb, Croatia*

[p] *Université Paris-Saclay, F-91191 Gif-sur-Yvette, France*

[q] *Physikalisches Institut, University of Bonn, Nußallee 12, 53115 Bonn, Germany*

[1]Corresponding author.

[2]Now at Gran Sasso Science Institute, Viale F. Crispi, 7 67100 L'Aquila, Italy.

[3]Now at SOLEIL Synchrotron, L'Orme des Merisiers, Départementale 128, 91190 SaintAubin, France.

[4]Now at Department of Particle Physics and Astronomy, Weizmann Institute of Science, Rehovot, 7610001, Israel.

[5]Now at TÜV NORD EnSys GmbH Co. KG.

[r] *Friedrich-Alexander-Universität Erlangen-Nürnberg, Schloßplatz 4, 91054 Erlangen, Germany*

[s] *CEA-LIST, Diamond Sensors Laboratory, CEA Saclay, F-91191 Gif-sur-Yvette, France*

[t] *Center for Interdisciplinary Research and Innovation (CIRI-AUTH), Thessaloniki 57001, Greece*

[u] *State Key Laboratory of Solid Lubrication, Lanzhou Institute of Chemical Physics, Chinese Academy of Science, Lanzhou 730000, China*

[v] *National Technical University of Athens, Athens, Greece*

[w] *Ruđer Bošković Institute, Bijenička cesta 54, 10000 Zagreb, Croatia*

E-mail: zhouyi@mail.ustc.edu.cn

ABSTRACT: The PICOSEC Micromegas (MM) is a Cherenkov photodetector based on the MM detector operating in a two-stage amplification mode. Prototypes equipped with a cesium iodide (CsI) photocathode have shown promising time resolutions as low as 24 picoseconds (ps) for Minimum Ionizing Particles. However, due to the high hygroscopicity and susceptibility to ion bombardment of the CsI photocathode, alternative photocathode materials such as pure aluminum, pure chromium, as well as Diamond-like Carbon (DLC) have been studied to improve the robustness of detector. Among these, DLC has yielded the most favorable results. A batch of DLC photocathodes with different thicknesses were produced and evaluated by using ultraviolet light and particle beam. The results of both quantum efficiency measurement and beam test indicate that the optimized thickness of the DLC photocathode is approximately 3 nm. The PICOSEC MM prototype equipped with a 3 nm DLC photocathode has reached a time resolution of around 42 ps with a detection efficiency of 97% for 150 GeV/c muons. Furthermore, the DLC photocathodes have shown good resistance to ion bombardment in the aging test compared to CsI photocathode. These results confirm the great potential of DLC as a photocathode for the PICOSEC MM detector.

KEYWORDS: Micropattern gaseous detectors (MSGC, GEM, THGEM, RETHGEM, MHSP, MICROPIC, MICROMEGAS, InGrid, etc), Timing detectors, Photocathodes and their production, Cherenkov detectors

Contents

1　Introduction

The development of a new generation of particle detectors with precise timing performance has been driven by the challenging environments of future High Energy Physics experiments, including severe pile-up effects in the upgraded High Luminosity Large Hadron Collider. Time resolution on the order of tens of picoseconds (ps) is required, as well as long-term stability, robustness and large area coverage[1, 2]. The study of detectors based on micro-pattern gaseous detectors (MPGDs) is very attractive since the advantages of MPGDs, including high-rate capability, radiation resistance and the ability to cover large area at low cost. A gaseous detector with precise timing performance has a wide range of applications, such as time-of-flight measurement, particle identification and suppression of pile-up effects in high luminosity environments[3, 4].

The detection concept of PICOSEC Micromegas (MM), which is based on a two-stage MM structure and Cherenkov radiation detection, was indeed proposed in 2015[5]. As shown in figure 1a, a Cherenkov radiator (3 mm MgF_2) coated with a photocathode, consisting of 18 nm Cesium Iodide (CsI) and 3.3 nm metallic bases, is coupled to the MM. Ultraviolet (UV) photons are generated when a charged particle passes through the radiator, and then the photoelectrons (PEs) will be extracted simultaneously from the photocathode. Due to the high electric field applied between the photocathode and mesh, the PEs are first multiplied in the pre-amplification gap. Then, a portion of the avalanche electrons can traverse the mesh and are further amplified in the amplification gap. The PICOSEC MM prototype studied in this paper was operated with the gas mixture of 80% Ne, 10%

C_2H_6, 10% CF_4. For the first PICOSEC MM prototype, a time resolution of 24 ps at a mean yield of 10.4 PEs with CsI photocathode has been measured for 150 GeV/c muon beam at the CERN SPS H4 secondary line[6]. However, due to the high electric field in the pre-amplification gap, substantial feedback ions bombard the CsI photocathode, causing an aging problem[7]. Figure 1b shows the microscopic image of the CsI photocathode after beam test data acquisition. It is noticeable that there is a mesh projection due to ion impacts, along with the presence of circular area attributed to the pillars of MM. Another degeneration issue is the cracks on the CsI layer caused by the sparks occurring within the gap. Additionally, a dry environment is required for storage and operation due to its hygroscopic and deliquescent nature[8, 9].

Alternative photocathodes with a chemical stability, resistance to ion bombardment, and suitable quantum efficiency (QE) are required for long-term operation of the PICOSEC MM. Within the PICOSEC MM collaboration, various candidates have been studied, including pure metallic (aluminum or chromium) photocathode, nano-diamond based photocathode, Diamond-like Carbon (DLC) photocathode as well as CsI photocathode with protection layer. Among these, the DLC photocathode has shown the most promising results. In this paper, we focus on the study of the DLC photocathode. The magnetron sputtering technology used to fabricate the DLC photocathode is described in section 2. Subsequently, the UV light and charged particles are used to study the characteristics of DLC photocathode and the performance of PICOSEC MM prototype with DLC photocathode, as detailed in section 3. The last section is a summary drawn from this paper.
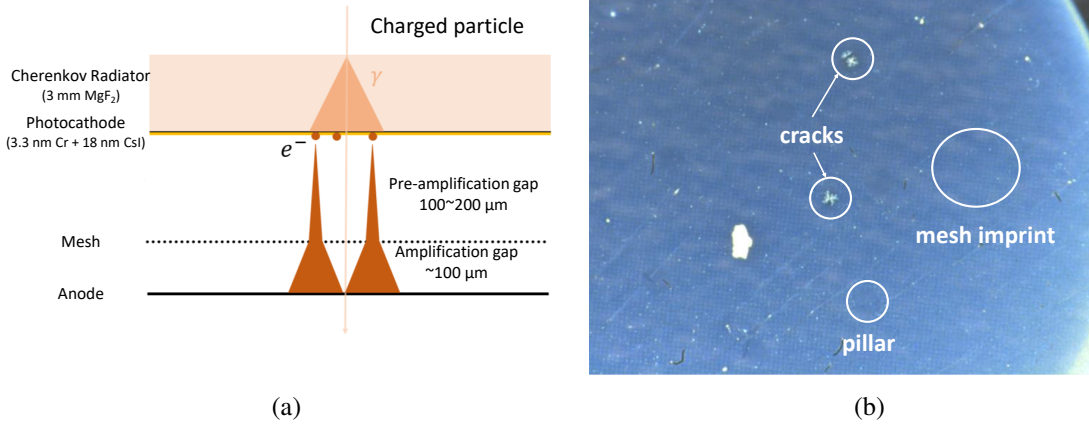

(a) (b)

Figure 1: Schematic view of PICOSEC MM detection concept (a). The microscopic image of CsI photocathode after beam test (b)

2 Production of DLC photocathode

Diamond film can be employed for the detection of UV photons with reasonable sensitivity, without significant problems of aging and radiation damage[10]. Based on this, we proposed DLC as the photocathode material for PICOSEC MM. DLC is a kind of novel resistive material with metastable amorphous structures containing both diamond-structure and graphite-structure carbon atoms[11],

as shown in figure 2. It has excellent electrical properties and suitable sensitivity, as well as chemical stability and thermal stability.
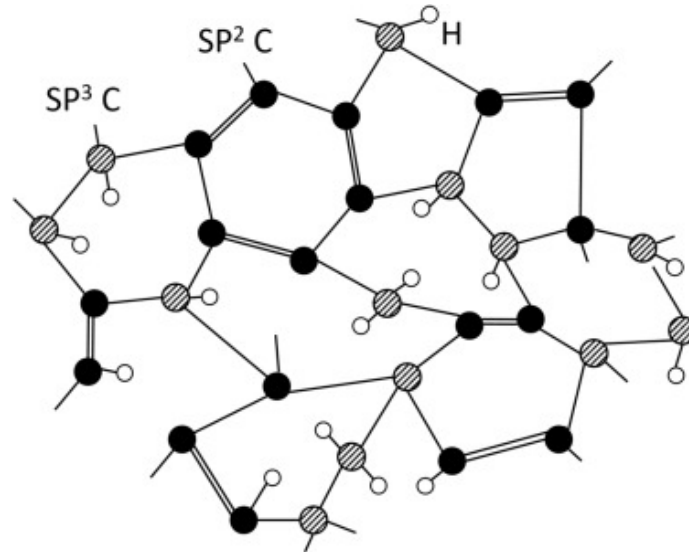

Figure 2: The atom structure of DLC, which contains both sp^3 (diamond-structure) and sp^2 (graphite-structure)

The magnetron sputtering technology[12] is an effective method for DLC deposition at low temperature. It provides a deposition process with good reproducibility and control, ensuring accuracy for the thickness and uniformity of the DLC film. The DLC film is directly deposited onto the surface of the MgF$_2$ crystal to form the DLC photocathode. A schematic diagram of the deposition process is illustrated in figure 3. Several permanent magnets are arranged on the back side of the graphite target to produce closed magnetic field lines around the surface of target. Before commencing the deposition process, the sputtering chamber is evacuated to the preset vacuum level, afterward argon is filled into the chamber. As the bias voltage between the substrate and the target ramps up, glow discharges occur and produce primary electrons. These primary electrons are accelerated by the electric field and ionize the argon molecules into ions and secondary electrons. The argon ions are accelerated in the field, then bombard the target and sputter out a number of carbon atoms or clusters. These sputtered carbon atoms or clusters are then deposited onto the surface of the substrate, forming a thin film. The secondary electrons are bounded inside the plasma region near the target surface by the Lorentz force of the magnetic field. Continuously ionizing the argon molecules, they producing argon ions that further bombard the target.

The coating machine we used is Teer650 (Teer Coating Ltd) at Lanzhou Institute of Chemical Physics. During the coating process, the MgF$_2$ crystal is fixed in the aluminum holders before being positioned within the chamber, as shown in figure 4a. The coating vacuum is maintained at a level better than 1×10^-6 Torr. A series of DLC photocathodes with the film thicknesses varying from 1 nm to 10 nm were produced by adjusting the deposition time while keeping other conditions constant. As shown in figure 4b, the DLC film, which is marked with four black dots, is deposited on a 3 mm thick MgF$_2$ crystal.
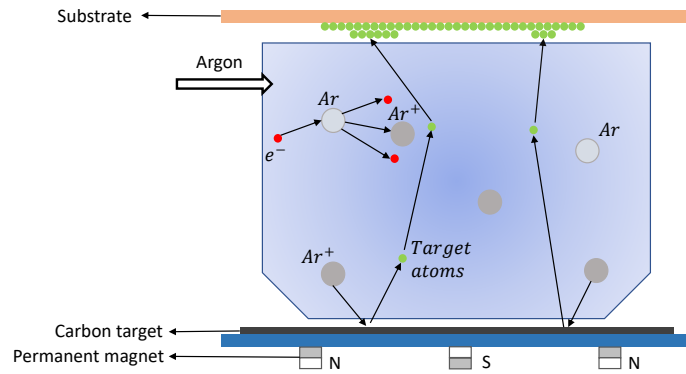
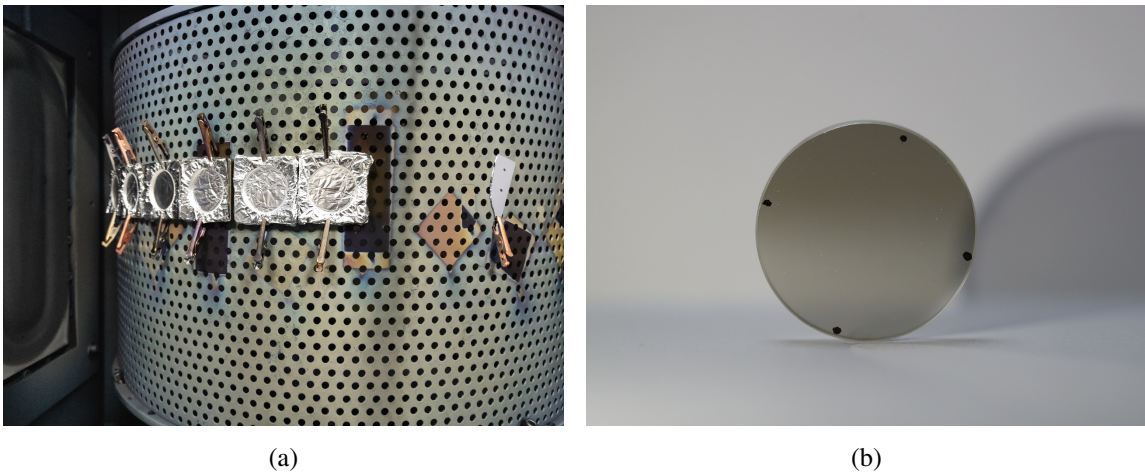**Figure 3**: Schematic diagram of DLC deposition by the magnetron sputtering technology

Figure 4: MgF$_2$ crystals are fixed in the coating chamber (a) and a sample of DLC photocathode (b)

3 Experiment study of DLC photocathode

3.1 QE measurement

3.1.1 Setup

The QE performance of DLC photocathodes was measured using a vacuum ultraviolet (VUV) QE test platform (ASSET), developed by the Gaseous Detectors Development Group (GDD) at CERN. The transmission QE measurement function of this device was used. A VUV monochromator (McPherson 234/302) is used to select the wavelength of the UV photons produced by a deuterium lamp from 120 nm to 200 nm with an accuracy of 0.1 nm. The UV photons are split into two beams by a beam splitter. One of them irradiates on a photomultiplier tube (ET-enterprises 9403B) (PMT$_1$), while the other one enters a measurement chamber and directly irradiates on another PMT (PMT$_2$) or passes through the sample to be measured.

Figure 5 illustrates the two steps involved in the QE measurement using ASSET. As a first step, two PMTs are used to measure the intensity of two beams without photocathode in the light path at
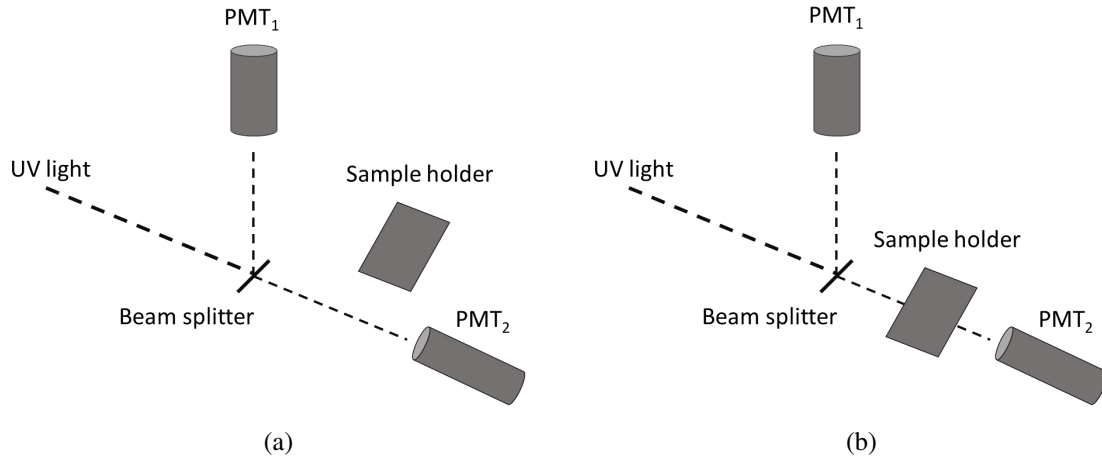
Figure 5: Schematic diagram of the two steps of QE measurement

a given wavelength. Picoammeters (Keithley model 6482) are used to measure the current from the two PMTs, current I_{ref0} from PMT_1 and I_{abs0} from PMT_2 are recorded. Then, in the second step, a holder containing the photocathode and wire electrode, as shown in figure 6, is placed in the light path in front of the PMT_2 within the measurement chamber. A suitable voltage is applied to the wire electrode to establish an electric field between the wire electrode and the photocathode for PEs emission and collection. During this step, the picoammeter connected to the DLC film measures the photocurrent (I_{pe}) generated by the PEs emissions when the UV photons pass through the MgF_2 crystal and irradiate on the DLC film. The number of photoelectrons (N_e) emitted per second is calculated by dividing I_{pe} by the charge of electron. At the same time, the current (I_{ref1}) generated from PMT_1 is recorded. The QE of the DLC photocathode can be obtained using the following formula:

$$QE = \frac{N_e}{N_p} = \frac{\frac{I_{pe}}{e}}{A \times I_{ref1} \times \frac{I_{abs0}}{I_{ref0}}} \tag{3.1}$$

Where N_p is the number of photons per second, e is the charge of electron and A is the response coefficient of PMT_1 to UV photons. In this case, the QE results contain the effects of MgF_2 crystal.

3.1.2 Results

In this measurement, DLC photocathodes with different thicknesses are measured and the relative QE were compared. The QE results of QE are shown in figure 7, which corresponding to 3 nm, 5 nm, 7.5 nm and 10 nm, respectively. All of the results are normalized by using the QE value for the DLC photocathode of 10 nm that measured at the wavelength of 130 nm. The results indicate that the optimized thickness of the DLC photocathode is 3 nm and the QE value is the highest under 130 nm UV photons irradiation. Besides, attempts were made to produce and measure a thinner layer (about 1 nm) to further enhance the performance. However, both the production and QE measurements were not reliable, and the thinner layer was found lacked sufficient resistance for storage and operation.
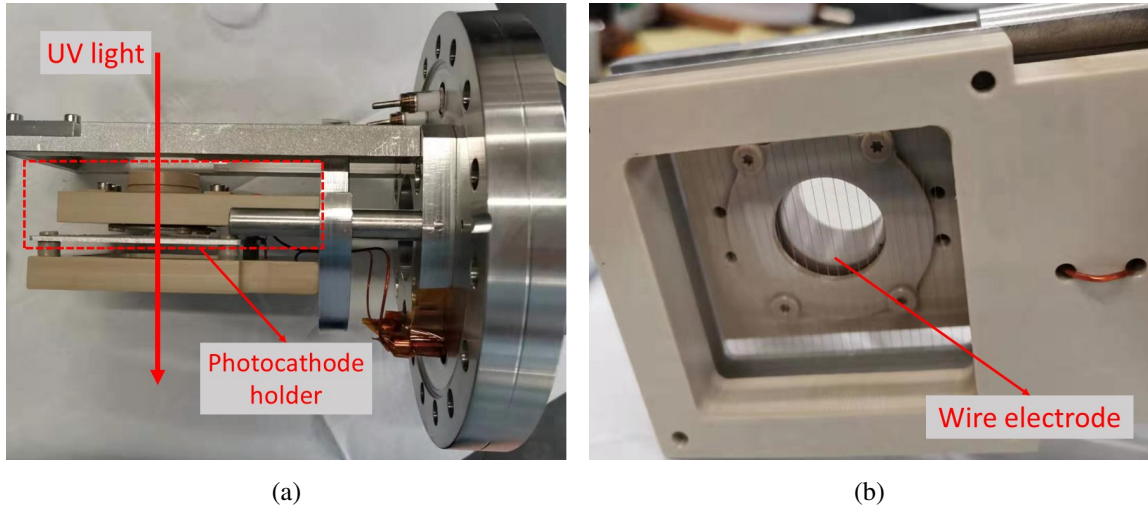
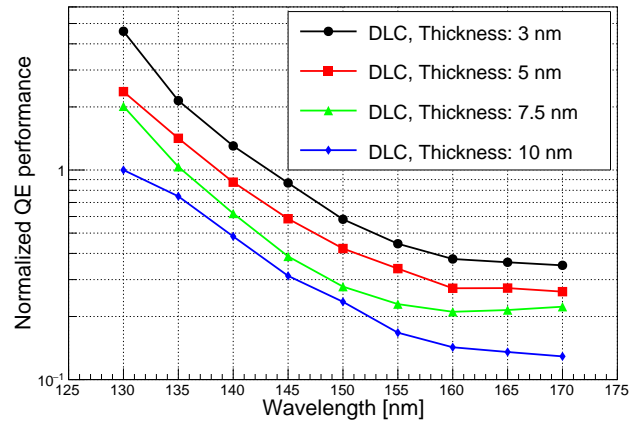Figure 6: Pictures of the photocathode holder and wire electrode of ASSET

Figure 7: Normalized QE performance of different DLC photocathodes

The transmissive QE measurement in ASSET only reflects the performance of the DLC photocathode when UV photons are incident, whereas the PICOSEC MM detector is more concerned with the performance when charged particles are incident. Therefore, we have performed tests on these photocathodes in a particle beam to evaluate their performance in a near-application environment.

3.2 Beam test

3.2.1 Setup

Beam tests for the PICOSEC MM prototype were carried out at the CERN SPS H4 secondary line. A 150 GeV/c muon beam was used to measure the performance of the PICOSEC MM prototype equipped with different DLC photocathodes. The exploded view of the prototype is shown in figure 8a. A bulk MM with a typical amplification gap of 128 μm is employed for electron multiplication and signal readout[13]. Its effective area is 1 cm in diameter. Several support rings

are used to form a 200 μm pre-amplification gap between the photocathode and the mesh. A current amplifier (CIVIDEC 2 GHz) was used to amplify the signal from the anode.
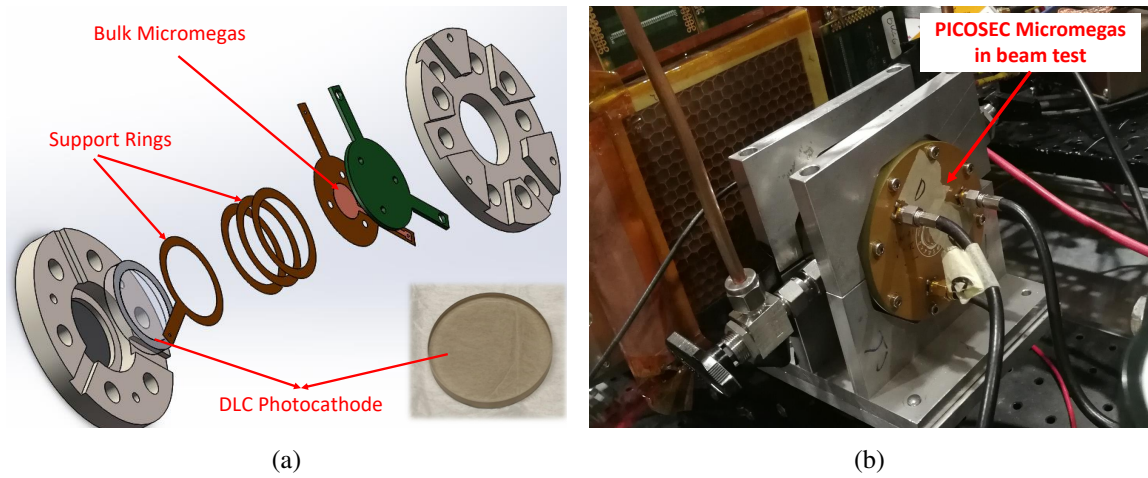

(a)

(b)

Figure 8: The design and picture of a single pad PICOSEC MM prototype

The setup of beam telescope is shown in figure 9. The prototype equipped with various photocathodes is placed in a test platform that provides accurate tracking and timing reference, as shown in figure 8b. Three triple-GEMs were used to provide precise tracking information of muons, and a multiple micro-channel plate photomultiplier tube (MCP-PMT, model Hamamatsu R3809U-50) was used as the time reference which providing a time resolution of better than 6 ps[14]. The active area of MCP-PMT is 11 mm in diameter, which is aligned with the anode electrode of the PICOSEC MM prototype. In the data acquisition, the signals of both the PICOSEC MM prototype and the MCP-PMs are recorded with an oscilloscope (20 Gsps and 4 GHz bandwidth).
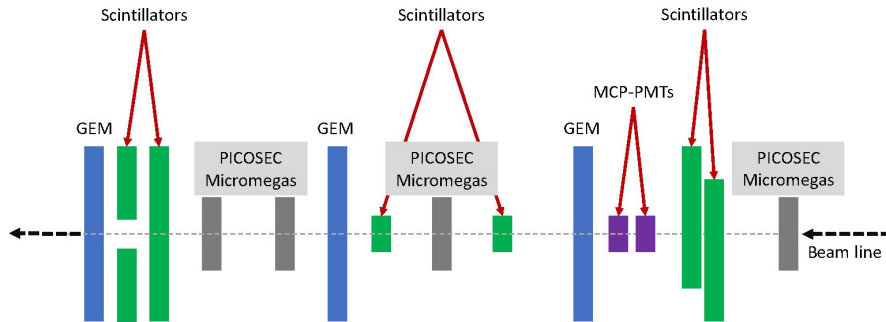

Figure 9: Sketch of the beam telescope

Firstly, the number of PEs extracted from the photocathode per muon incident (N_{pe}/μ) was tested. The yield of PEs is closely related to the QE of the photocathode, which is the crucial performance of the photocathode. In the beam condition, this number is estimated from the response of the muon beam and a single PEs calibration using a UV lamp at the same voltage. In addition, the time resolution of the prototype with different DLC photocathodes was studied to reach the optimized time performance. The time information of the prototype and the MCP-PMT

Table 1: PEs yield results of different DLC photocathodes

Thickness of DLC film (nm)	N_{pe}/μ	Detection efficiency
3	3.7	97%
5	3.4%	94%
7.5	2.2%	70%
10	1.7%	68%

was obtained by fitting the leading edges with a sigmoid function and performing 20% constant fraction discrimination (CFD). The time difference between the MCP-PMT and the prototype is defined as the "signal arrival time" (SAT). The time resolution (σ) of the prototype, which contains the contribution of the MCP-PMT and other effects, can be acquired by fitting the distribution of the SAT with a Gaussian function. This methods are described detailed in [6, 15]. Both the results of the yield of the DLC photocathodes and the time resolution of the prototype are detailed in the following sections.

3.2.2 PEs yield

For the prototype, the amplitude distributions of the signal from single PEs and muon beam were fitted using a polya function[15–17]. The mean amplitude of single PEs and muons were denoted as Q_e and Q_{mu}, respectively. The PEs yield is simply estimated by dividing Q_{mu} by Q_e. For DLC photocathodes, the results are shown in Table 1. When the thickness of DLC film is 3 nm, the optimal performance is obtained, for which the yield is approximately 3.7 N_{pe}/μ. By comparing all the photocathodes, it can be seen that as the thickness of the DLC film increases from 3 nm to 10 nm, the PEs yield decreases, which is consistent with the results of QE measurement. Additionally, under the same conditions, an 18 nm CsI photocathode was also tested, while the yield was approximately 10 N_{pe}/μ[6].

The more PEs extracted from the photocathode, the higher the detection efficiency will be obtained. As the thickness of the DLC film increases from 3 nm to 10 nm, the detection efficiency of the prototype for charged particles decreases from 97% to 68%, while the detection efficiency approaches 100% when using CsI photocathode. These results indicate that using a 3 nm DLC photocathode, the PICOSEC MM prototype can maintain sufficient detection efficiency for charged particles.

3.2.3 Time resolution

The time resolution of the prototype equipped with different types of DLC photocathode was tested. Of these, the 3 nm DLC photocathode exhibits the best performance, followed by the 5 nm, 7.5 nm and 10 nm photocathodes in descending order of performance, which is consistent with the results of PEs yield and QE. Figure 10a and 10b show the time resolution of the prototype equipped with 3 nm and 10 nm DLC photocathodes, respectively. It can be clearly seen that the time resolution improves with higher pre-amplification voltage, which has the same tendency when using CsI photocathode. With the 3 nm DLC photocathode, the time resolution reached up to approximately 42 ps at the voltage of 550 V of pre-amplification gap and 300 V of amplification gap. With the thickness of the

DLC film increases, the time resolution deteriorated. With the 10 nm DLC photocathode, the best time resolution was only about 76 ps, even higher voltage on pre-amplification gap was applied.
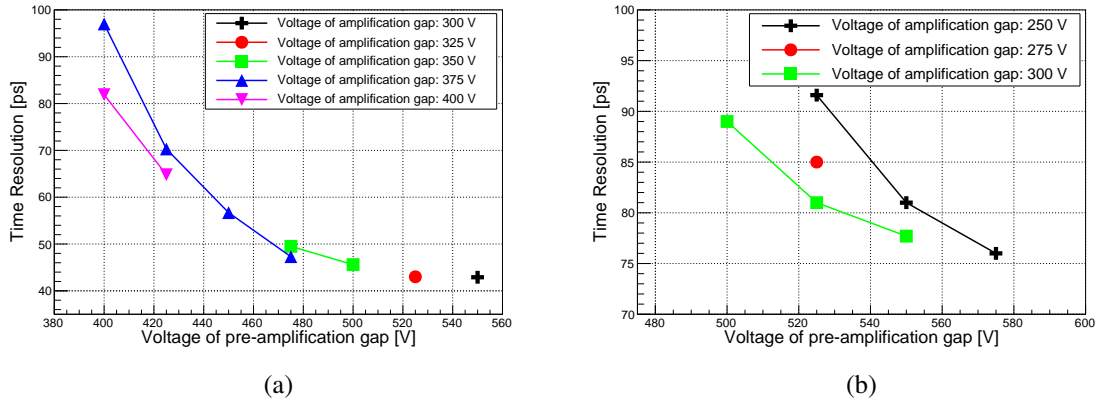

Figure 10: Time resolution results of the PICOSEC MM prototype equipped with a 3 nm and 10 nm DLC photocathode

As a comparison, the time resolution of the prototype with an 18 nm CsI photocathode was also tested at the same voltage. A time resolution of approximately 28 ps was obtained when the voltage of pre-amplification gap and amplification gap were 550 V and 300 V, respectively. Due to the high PEs extraction efficiency of the CsI photocathode, the prototype can achieve better time resolution compared to the DLC photocathode. However, the robustness of the DLC photocathode is a significant advantage compared to CsI photocathode. As a compromise between time resolution and detector's operation time, DLC photocathode demonstrates the potential to be the most promising candidate. The aging effect of the DLC photocathode was also studied, as well as that of the CsI photocathode, which is shown in the next section.

3.3 Aging test

3.3.1 Setup

At the typical operating point of the PICOSEC MM, the ratio of ions feedback to the position of photocathode is huge, which will cause non-negligible damage to the CsI photocathode. To verify the resistance of the DLC photocathode to ion bombardment, aging test with high intensity laser was carried out. The test setup is shown in figure 11. A pulsed laser (Passat Lat. Compiler-213) was used to provide laser with a wavelength of 213 nm. The laser beam is split into two beams. One beam line is recorded by a laser energy meter (COHERENT PM10) which is used to monitor the stability of the laser intensity. The other beam line is sent to the prototype for aging study of the photocathodes. The positive voltage is applied to the anode and mesh electrode, while the photocathode is maintained at 0 V and connected to a picoammeter (Keithley model 6487). The voltage of pre-amplification gap and the amplification gap are set to 420 V and 300 V, respectively. The prototype maintains a constant gain by keeping the voltage and other factors fixed.

In the test, when the prototype is exposed to the UV laser, the photocathode promptly responds by emitting primary PEs, a direct consequence of the photoelectric effect. These PEs are then
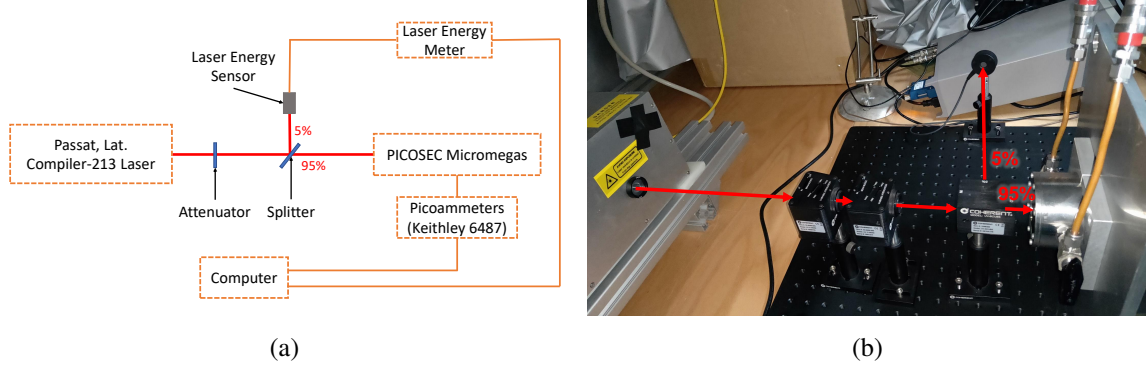
Figure 11: Schematic diagram and picture of aging test using UV laser

further ionized and multiplied in the gas gap, while the ions generated during the ionization process feedback to the position of photocathode and bombard the photocathode film. With the continuous irradiation of laser, the current of feedback ions $I(t)$ from the photocathode and the laser intensity $P(t)$ were simultaneously recorded by the picoammeter and the laser energy meter. Since the gas gain remains unchanged, the normalized current $I(t)/P(t)$ can be used as an indicator of the photocathode's QE performance. Additionally, the number of charges accumulated on the photocathode can be obtained by integrating the current $I(t)$. The visible degeneration area of the CsI photocathode after aging test was investigated under a microscope, and an irradiated area of approximately $0.06\,\mathrm{cm}^2$ was obtained. This area differs from the one indicated in the manual, which is a cycle with a diameter of 2.5 mm, due to the distortion caused by the laser passing through the optics and the window of the prototype.

3.3.2 Results

The test results are shown in figure 12, where the x-axis is the accumulated charge on the photocathode, and the y-axis is the normalized QE performance of the photocathode. The three curves in figure. 11 represent one CsI photocathode and two DLC photocathodes, with the thicknesses of 18 nm (black curve), 3 nm (blue curve) and 5 nm (red curve), respectively. For each curve, the first data point is normalized to 1. As can be seen from the plot, the performance of the CsI photocathode drops rapidly to around 30% after being bombarded by ions of around 10 mC/cm^2. However, the DLC photocathodes, they can maintain stable QE performance after a slight deterioration. When the accumulated ions on the DLC photocathodes reach tens of mC/cm^2, or even exceed 100 mC/cm^2, their performance degradation is less than 20%. Furthermore, the damaged region of the CsI photocathode after aging can be clearly seen under the microscope, which corresponds to the laser irradiation area, but it is very difficult to find marks on the DLC photocathodes when they are bombarded with even more feedback ions. These results indicate that the PICOSEC MM detector with DLC photocathode can operate longer with stable performance than with CsI photocathode.

4 Conclusion

The DLC photocathode for the PICOSEC MM detector is introduced, and it has shown promising results with its suitable sensitivity and stability. Its performance is optimized through the manufac-
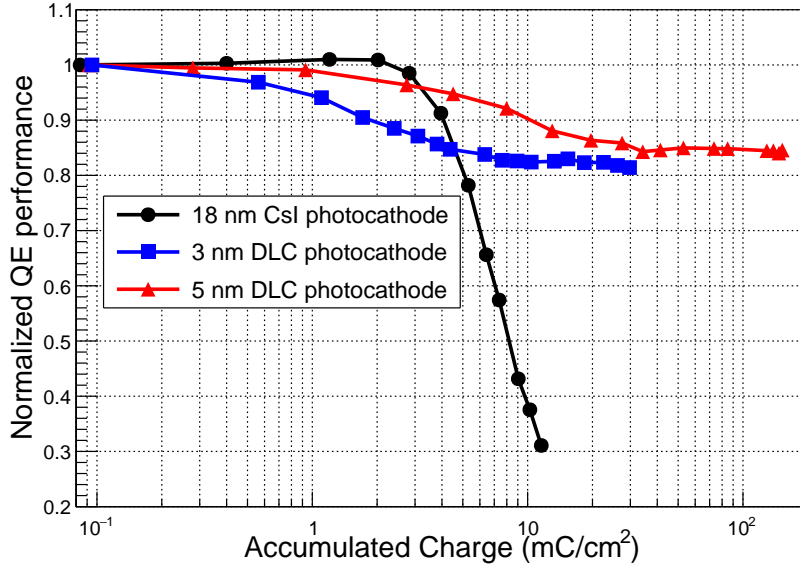
Figure 12: Dependence of the normalized QE performance on the accumulated charges for different photocathodes

turing processes, QE measurement and beam test. In the QE measurement, samples with different thickness are studied, and the results indicate that the optimized thickness of DLC photocathode is approximately 3 nm. Besides, charged particle beam is used to test the PICOSEC MM prototype equipped with DLC photocathode to verify its performance in practical application environment. A time resolution of around 42 ps with a detection efficiency of 97% for 150 GeV/c muons are obtained when the prototype equipped with a 3 nm DLC photocathode. The results in beam test agree well with those of the QE measurement. Additionally, the aging effect of ion bombardment was also tested. The two tested DLC photocathodes maintain stable QE performance after a slight decrease, which is less than 20%, after being bombarded with feedback ions of around 100 mC/cm^2. As a comparison, the CsI photocathode has shown rapid damage when only 10 mC/cm^2 is accumulated on the CsI film. In conclusion, the good properties of no hydrolysis, chemical stability and robustness to ion bombardment of the DLC photocathode demonstrate its great application potential as the photocathode for the PICOSEC MM detector.

Acknowledgments

References

[1] S. White, *Experimental challenges of the european strategy for particle physics*, *arXiv preprint arXiv:1309.7985* (2013) .

[2] E. Group et al., *The 2021 ecfa detector research and development roadmap*, Tech. Rep. Tech. rep., Geneva (2020).

[3] S. Chekanov, A. Kotwal, C.-H. Yeh and S.-S. Yu, *Physics potential of timing layers in future collider detectors*, *Journal of Instrumentation* **15** (2020) P09021.

[4] J. Va'vra, *Pid techniques: Alternatives to rich methods*, *Nuclear Instruments and Methods in Physics Research Section A: Accelerators, Spectrometers, Detectors and Associated Equipment* **876** (2017) 185.

[5] T. Papaevangelou, D. Desforge, E. Ferrer-Ribas, I. Giomataris, C. Godinot, D.G. Diaz et al., *Fast timing for high-rate environments with micromegas*, in *EPJ Web of Conferences*, vol. 174, p. 02002, EDP Sciences, 2018.

[6] J. Bortfeldt, F. Brunbauer, C. David, D. Desforge, G. Fanourakis, J. Franchi et al., *Picosec: Charged particle timing at sub-25 picosecond precision with a micromegas based detector*, *Nuclear Instruments and Methods in Physics Research Section A: Accelerators, Spectrometers, Detectors and Associated Equipment* **903** (2018) 317.

[7] X. Wang, "R&D for fast timing detector based on micromegas." in: The 10th Conference of High Energy Physics of China, June, 2018.

[8] Y. Xie, A. Zhang, Y. Liu, H. Liu, T. Hu, L. Zhou et al., *Influence of air exposure on csi photocathodes*, *Nuclear Instruments and Methods in Physics Research Section A: Accelerators, Spectrometers, Detectors and Associated Equipment* **689** (2012) 79.

[9] V. Razin, Y.N. Gotovcev, A. Kurepin and A. Reshetin, *The influence of exposure to air on the quantum efficiency of thin csi photocathodes*, *Nuclear Instruments and Methods in Physics Research Section A: Accelerators, Spectrometers, Detectors and Associated Equipment* **419** (1998) 621.

[10] M. Nitti, M. Colasuonno, E. Nappi, A. Valentini, E. Fanizza, F. Bénédic et al., *Performance analysis of poly-, nano-and single-crystalline diamond-based photocathodes*, *Nuclear Instruments and Methods in Physics Research Section A: Accelerators, Spectrometers, Detectors and Associated Equipment* **595** (2008) 131.

[11] A. Grill, *Diamond-like carbon: state of the art*, *Diamond and related materials* **8** (1999) 428.

[12] P.J. Kelly and R.D. Arnell, *Magnetron sputtering: a review of recent developments and applications*, *Vacuum* **56** (2000) 159.

[13] I. Giomataris, R. De Oliveira, S. Andriamonje, S. Aune, G. Charpak, P. Colas et al., *Micromegas in a bulk*, *Nuclear Instruments and Methods in Physics Research Section A: Accelerators, Spectrometers, Detectors and Associated Equipment* **560** (2006) 405.

[14] L. Sohl, *Spatial time resolution of mcp-pmts as a t0-reference*, *Nuclear Instruments and Methods in Physics Research Section A: Accelerators, Spectrometers, Detectors and Associated Equipment* **936** (2019) 583.

[15] L. Sohl, *Development of PICOSEC-Micromegas for fast timing in high rate environments*, Ph.D. thesis, Université Paris-Saclay, 2020.

[16] H. Schindler, *Microscopic simulation of particle detectors*, Ph.D. thesis, CERN, 2012.

[17] T. Zerguerras, B. Genolini, F. Kuger, M. Josselin, A. Maroni, T. Nguyen-Trung et al., *Understanding avalanches in a micromegas from single-electron response measurement*, *Nuclear Instruments and Methods in Physics Research Section A: Accelerators, Spectrometers, Detectors and Associated Equipment* **772** (2015) 76.